LANGMUIR

Article

pubs.acs.org/Langmuir

Scanning Electrochemical Microscopy Study of Permeability of a Thiolated Aryl Multilayer and Imaging of Single Nanocubes Anchored to It

Pierre-Yves Blanchard,[†] Tong Sun,[†] Yun Yu,[†] Zengyan Wei,[‡] Hiroshi Matsui,*[,‡,§] and Michael V. Mirkin*[,†]

[†]Department of Chemistry and Biochemistry, Queens College and the Graduate Center, City University of New York (CUNY), Flushing, New York 11367, United States

[‡]Department of Chemistry and Biochemistry, Hunter College and the Graduate Center, City University of New York (CUNY), New York, New York 10021, United States

[§]Department of Biochemistry, Weill Medical College of Cornell University, New York, New York 10021, United States

Supporting Information

ABSTRACT: Electroreduction of diazonium salts is a widely used technique for grafting organic films on various surfaces. In this paper, scanning electrochemical microscopy (SECM) was used for high-resolution characterization of a thiolated aryl multilayer film obtained by electrografting of thiophenol diazonium on highly ordered pyrolytic graphite (HOPG). The blocking properties of the film were evaluated, and the origins of incomplete surface passivation were elucidated by comparing current−distance curves and surface reactivity maps obtained with nanometer- and micrometer-sized tips. In this way, one can distinguish between different pathways of charge transport in the film, e.g., pinhole defects versus rate-limiting charge transfer through the film. Pd nanocubes were anchored to the film by thiol groups and imaged by SECM. The applicability of SECM to *in situ* visualization of the geometry of non-spherical nanoparticles has been demonstrated.

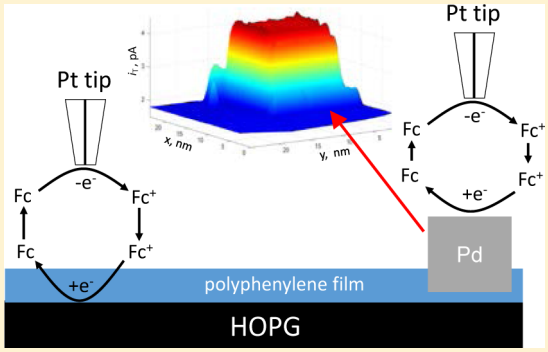

INTRODUCTION

Since the pioneering work of the Savéant group,[1] the surface modification via electroreduction of diazonium salts has been the focus of considerable research activity.[2] This approach offers important advantages, including its high efficiency, robustness and chemical stability of the produced films, flexible strategies, and applicability to diverse substrates. The possibility of using diazonium cations with different substituent groups enables the preparation of surfaces with broad chemical and/or physical properties. The covalently bonded films are potentially useful for corrosion protection,[3] nanoelectronics,[4] sensors,[5] and energy storage.[6]

The attachment of an aryldiazonium film passivates the substrate and significantly decreases the electron transfer (ET) rate between its surface and the redox species in solution, as revealed by a decrease in the peak current and an increase in the peak potential separation in cyclic voltammograms (CVs). However, the origin and extent of the passivation remain controversial, and the published data are not consistent. The blocking properties are affected by such factors as the nature of solvent and electrolyte, pH value, film thickness[7] and compactness, and hydrophilic/hydrophobic interactions between the film and redox probe.[8] The Bélanger group[7] investigated the blocking effect of the electrografted 4-diazo-*N*,*N*-diethylaniline film on four different ET reactions as a function of solution pH and presented convincing evidence for the significance of the electrostatic repulsion. However, the blocking was very strong for $Fe(CN)_6^{3/4-}$ species and almost negligible for the faster $IrCl_6^{2/3-}$ couple, regardless of the film charge, thus pointing to the importance of the ET kinetics. At the same time, the very fast ET involving $Ru(NH_3)_6^{3/2+}$ was significantly inhibited at low solution pH. The very strong blocking effect of both electrografted[7] and spontaneously adsorbed[9] films on oxidation/reduction of $Fe(CN)_6^{3/4-}$ was attributed to surface sensitivity of this reaction involving chemisorption. This explanation is not entirely clear because strong adsorption of $Fe(CN)_6^{3/4-}$ on carbon surfaces has not yet been reported. Moreover, this reaction produces well-defined quasi-reversible voltammograms at nanometer-sized electrodes, which is not the case for processes involving adsorbed reactants or intermediates (e.g., oxygen reduction reaction or dopamine oxidation).

Another open question is about the mechanism of the charge transport across the diazonium film, whose typical thickness of

Received: October 17, 2015
Revised: February 8, 2016
Published: February 29, 2016

ACS Publications © 2016 American Chemical Society

DOI: 10.1021/acs.langmuir.5b03858
Langmuir 2016, 32, 2500−2508

a few nanometers[10] (or more[11]) is too large for direct electron tunneling. The proposed pathways include electron hopping[12] and mediated charge transfer.[13,14] The charge propagation through various defects, including large (sub-micrometer) defects and pinholes (i.e., meso- or macropores[15]) has been suggested in several publications.[13−16] However, the direct evidence of pinholes [e.g., in atomic force microscopy (AFM) images[16]] is scarce,[2] and in most cases, their presence was inferred from electrochemical responses of the studied films. The reported effect of the redox probe hydrophobicity on the effective ET distance[8] pointed to the possibility of ion penetration into the multilayer.

The scanning electrochemical microscopy (SECM) methodologies have previously been developed to evaluate the mechanisms of charge-transfer processes at modified electrodes and measure the rates of charge/mass transport across the surface film.[17−23] In a feedback mode SECM experiment (Figure 1A), a micrometer- or nanometer-sized tip electrode

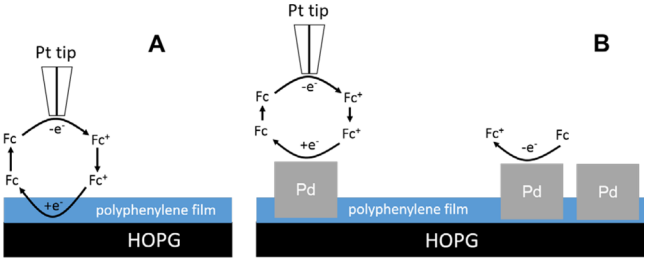

Figure 1. Schematic representation of the feedback mode SECM experiment at (A) HOPG substrate modified with a partially blocking aryldiazonium film and (B) Pd nanocube attached to this film.

approaches the aryldiazonium-modified substrate surface. The electrolyte contains an electroactive mediator [e.g., ferrocenemethanol (Fc)], and the tip potential (E_T) is such that the mediator oxidation (or reduction) occurs at a rate governed by diffusion. When the separation distance (d) becomes comparable to the tip radius (a), the oxidized form of the mediator (Fc^+) produced at the tip surface can be reduced at the substrate, producing the increase in the tip current (i_T) with decreasing d (positive feedback). The i_T can be recorded as a function of d (approach curve) or tip x−y position (imaging). If the mediator regeneration at the sample is too slow, the tip current decreases with decreasing d because of hindered diffusion of redox species (negative feedback). The smaller the tip, the faster the mass transfer in the tip/substrate gap, and the higher mediator regeneration rate at the substrate is required to produce a measurable positive feedback current.

It was shown previously[18,19] that an i_T versus d curve obtained with a tip approaching a partially blocked conductive substrate can be fitted to the SECM theory for finite heterogeneous kinetics at the substrate. The effective heterogeneous charge-transfer rate constant extracted from such a fit can be interpreted in the context of a specific mechanism of the interfacial ET and charge propagation across the film. For a partially blocking monolayer film containing no redox centers, the effective rate constant was presented as a combination of ET through the pinhole defects (k_{pin}) and direct tunneling (k_{direct})[19]

$$k_{eff} = k_{direct} + \theta_{pin} k_{pin} \quad (1)$$

where θ_{pin} is the fractional area of the pinholes in the film. In the case of a multilayer film, k_{direct} = 0, and eq 1 has to be modified, as discussed below.

SECM has been employed in quantitative studies of blocking properties of aryldiazonium films.[2,9,13−15] In addition to measuring the charge transfer through the film, SECM can provide spatially resolved information about variations in barrier properties and detect defects. The previously reported experiments were carried out with micrometer-sized SECM tips that were too large for detecting nanoscale pinholes. In this paper, we employ nanoelectrode tips to improve the spatial resolution, increase the mass-transfer rate, and, thus, characterize the weak blocking effect that may not be apparent from microelectrode experiments (e.g., there was no appreciable difference between the approach curves obtained using a micrometer tip and $Ru(NH_3)_6^{3/2+}$ redox mediator at a glassy carbon substrate before and after its modification with aryldiazonium.[9])

We have recently employed aryldiazonium films for immobilizing spherical gold nanoparticles (AuNPs) on carbon surfaces.[24,25] The films showed very stable and uniform negative SECM feedback, and a positive feedback current produced by the nanoparticles was easy to measure against this background. Although the mediator regeneration at the diazonium-modified highly ordered pyrolytic graphite (HOPG) was slow,[24,25] those experiments were performed with an unbiased (i.e., floating) substrate and the extent of surface passivation was not evaluated.

Nanoscale lateral resolution of SECM makes it suitable for experiments at single nanoparticles.[26,27] Several groups employed hybrid techniques (i.e., SECM−scanning ion conductance microcopy (SICM)[28,29] and SECM−AFM[30,31]) for probing individual immobilized nanoparticles. The lateral resolution of SECM imaging in ref 24 was sufficiently high to obtain topographic images of 10 and 20 nm AuNPs. Later,[25] the methodology was developed for evaluating the radius of a spherical nanoparticle from SECM approach curves. Here, we show that SECM can also be used to evaluate the geometry of non-spherical nanoparticles, i.e., Pd nanocubes.

EXPERIMENTAL SECTION

Chemicals. Ferrocenemethanol (97%, Sigma-Aldrich) was sublimed before use. Potassium chloride (Sigma-Aldrich), sodium nitrite (99.999%, Alfa Aesar), potassium ferrocyanide(II) trihydrate (99%, Sigma-Aldrich), hexaammineruthenium(III) chloride (99%, Strem Chemicals), 4-aminothiophenol (≥99%, Sigma-Aldrich), and 4-aminobenzoic acid (≥99%, Sigma-Aldrich) were used as received. Aqueous solutions were prepared using deionized water from the Milli-Q Advantage A10 system (Millipore) equipped with Q-Gard T2 Pak, a Quantum TEX cartridge and a VOC pak. The total organic carbon (TOC) was <1 ppb. HOPG (ZYB grade) was purchased from K-Tek Nanotechnology.

Pd Nanocubes. Cetyltrimethylammonium bromide (CTAB)-capped Pd nanocubes with the edge length of ∼14 nm were synthesized in the Matsui's laboratory (Hunter College), as described previously.[32] The solutions of Pd nanocubes were stored at 0−5 °C.

Electrochemical Experiments. Voltammograms were obtained using a BAS 100B electrochemical workstation (Bioanalytical Systems). A three-electrode cell was employed for electrochemical measurements, including cyclic voltammetry and electrografting. The HOPG (∼0.2 cm^2 surface area) served as a working electrode with a 0.5 mm diameter Pt wire employed as a counter electrode and an Ag/AgCl wire reference. All experiments were carried out at room temperature (22−25 °C) inside a Faraday cage.

DOI: 10.1021/acs.langmuir.5b03858
Langmuir 2016, 32, 2500−2508

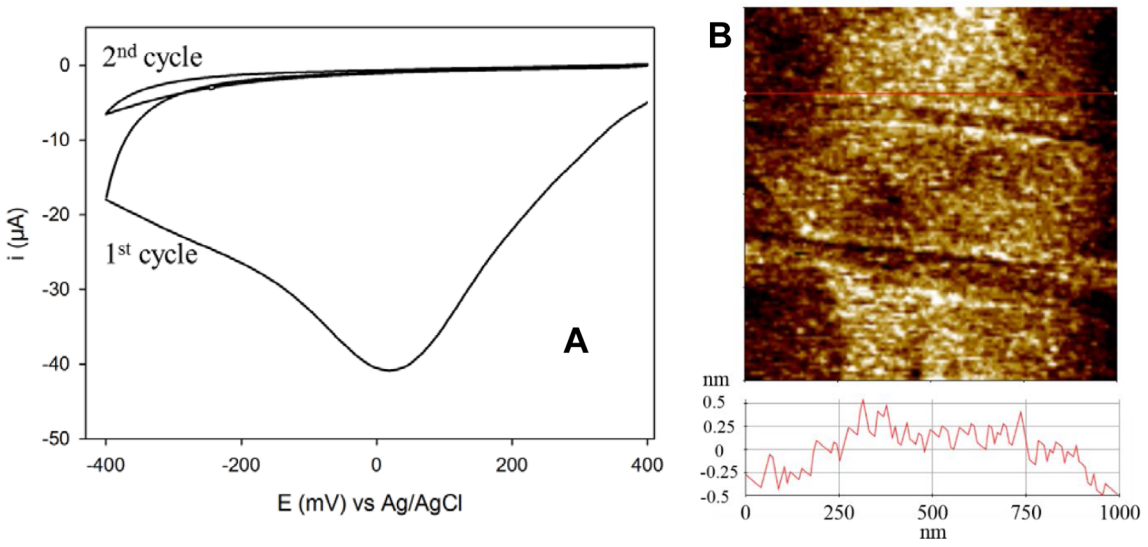

Figure 2. (A) CV of the formation of the TPD film obtained at a HOPG electrode in aqueous 0.5 M HCl solution containing 20 mM $NH_2-C_6H_4-SH$ and 40 mM $NaNO_2$ and (B) 1 × 1 μm^2 non-contact mode topographic AFM image of HOPG coated with the TPD film. The red line corresponds to the shown cross-section.

Scheme 1. Electrochemical Reduction of TPD and Film Grafting on the HOPG Electrode

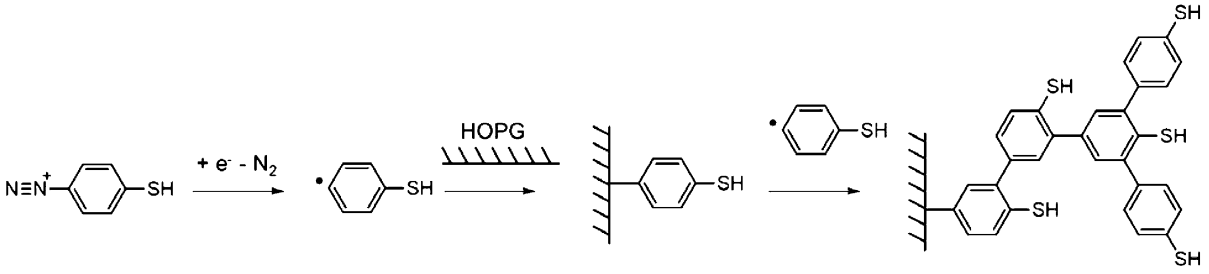

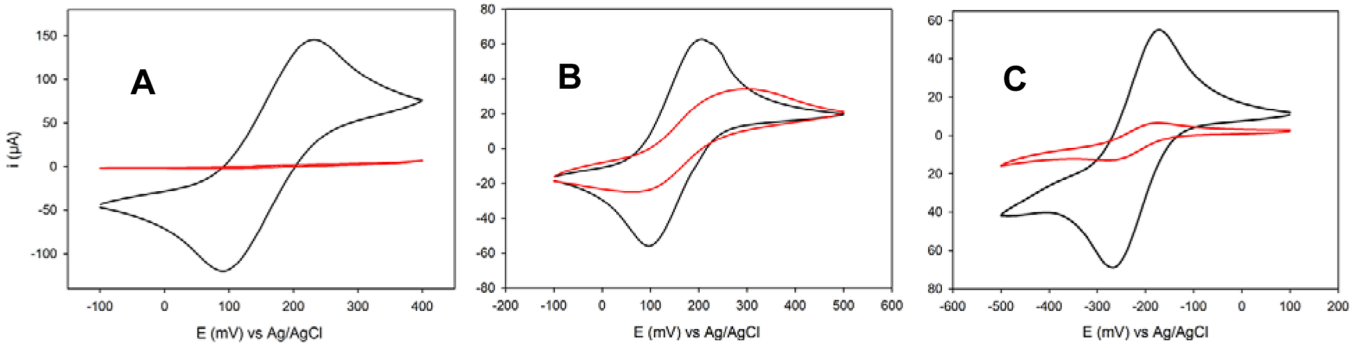

Figure 3. CVs of (A) 5 mM $K_4Fe(CN)_6$, (B) 1 mM Fc, and (C) 1 mM $Ru(NH_3)_6Cl_3$ obtained before (black) and after (red) modification of HOPG with TPD. Solutions contained 0.1 M KCl supporting electrolyte.

SECM Tips. Pt micro- and nanoelectrodes were fabricated as described previously.[33] Briefly, disk-type electrodes were prepared by pulling 25 or 50 μm diameter annealed Pt wires (Goodfellow) into borosilicate capillaries (Drummond; outer diameter, 1.0 mm; inner diameter, 0.2 mm) with the help of a P-2000 laser puller (Sutter Instrument Co.). The pulled nanoelectrodes were polished on a 50 nm alumina disk (Precision Surfaces International) under video microscopic control. The electrode radius was evaluated from AFM images and steady-state voltammograms. The RG value (i.e., the ratio of the glass insulator radius to that of the Pt disk) was between 6 and 15. Appropriate protection was used to avoid electrostatic damage to the nanotips.[34]

SECM Setup. SECM experiments were carried out using a home-built instrument, which was described previously.[24] To obtain an approach curve, the tip electrode was first positioned about 100 μm above the HOPG substrate. To avoid crashing, this process was monitored with a long-distance video microscope. Then, the tip was moved closer to the substrate in the automated "surface hunter" mode until the tip current produced by oxidation of Fc either increased (positive feedback) or decreased (negative feedback) by ~10%. The tip current was collected during the subsequent fine approach or imaging.

Surface Modification of HOPG. HOPG was freshly cleaved before each experiment using Scotch tape. Organic films were formed in 0.5 M HCl aqueous solution containing 20 mM 4-aminothiophenol and 40 mM (2 equiv) sodium nitrite. Figure 2A shows a CV of the reduction of *in situ* generated thiophenol diazonium (TPD). The CV shape is characteristic of the diazonium reduction, as reported

DOI: 10.1021/acs.langmuir.5b03858
Langmuir 2016, 32, 2500−2508

previously.[2] The first cycle represents the reduction of diazonium ion to aryl radical (Scheme 1). The subsequent covalent attachment of the radicals to the surface passivates it and greatly diminishes the faradaic current in the second cycle. The obtained film (Figure 2B) is a multilayer of disorganized benzene rings.[21]

To immobilize the Pd nanocubes, a 600 μL drop of solution containing the nanocubes was placed on the HOPG/TPD surface for 6 h. The substrate was then rinsed with water and imaged by AFM to check the density of nanocubes on the surface.

AFM, Scanning Electron Microscopy (SEM), and Transmission Electron Microscopy (TEM) Imaging. An XE-120 scanning probe microscope (Park Systems) with a PPP-NHCR probe was employed for non-contact imaging of modified HOPG, nanoparticles, and nanoelectrodes. The procedures for AFM imaging of nanoelectrodes were reported previously.[35]

TEM images were obtained using a JEOL 1200 EX transmission electron microscope. Pd nanocubes were dried onto a carbon-coated copper grid. SEM images of Pd nanoparticles on HOPG were obtained with a Zeiss Supra 55 VP scanning electron microscope with a 5 kV gun voltage.

RESULTS AND DISCUSSION

Charge Transfer across TPD Films. The barrier properties of the film were evaluated from CVs obtained at the HOPG

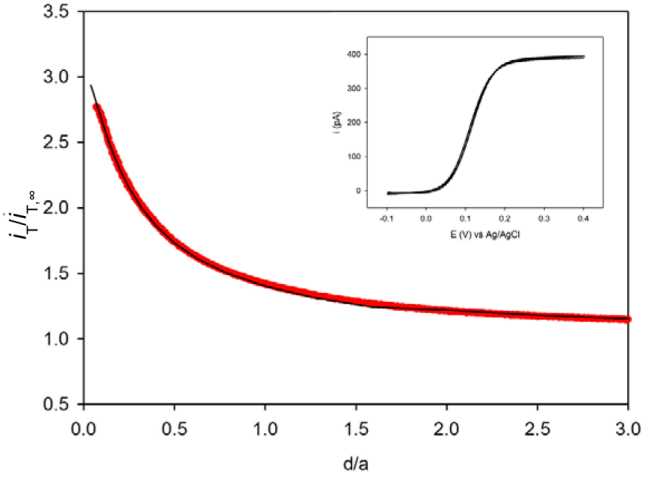

Figure 4. Experimental (symbols) SECM approach curve at the HOPG substrate modified with TPD obtained in 1 mM solution of Fc and fitted to the theory (solid curve[36]). E_S = −0.1 V, and E_T = 0.4 V. The inset shows CV of the Fc oxidation at the same tip electrode. Scan rate, v = 50 mV/s. a = 1.2 μm.

electrode before (black curves in Figure 3) and after (red curves in Figure 3) electrografting of TPD. The CVs in Figure 3 were obtained with three different redox mediators: (A) ferrocyanide, (B) Fc, and (C) hexaammineruthenium. In agreement with the literature data,[2] the ET between HOPG and $Fe(CN)_6^{3/4-}$ species was strongly inhibited by this electrically neutral film. The blocking effect of the film on much faster ET processes involving Fc^+/Fc or $Ru(NH_3)_6^{3/2+}$ was also significant. This is different from the previously reported experiments, where the oxidation/reduction of $Ru(NH_3)_6^{3/2+}$ was essentially unaffected by either electrografted[7] or adsorbed[9] neutral aryldiazonium films. In our experiments, the blocking effect of TPD films was stronger than that produced by electrografting of either aminomethylbenzenediazonium or carboxylbenzenediazonium.

More detailed information about surface passivation was obtained using SECM. With the ferrocyanide mediator, the ET

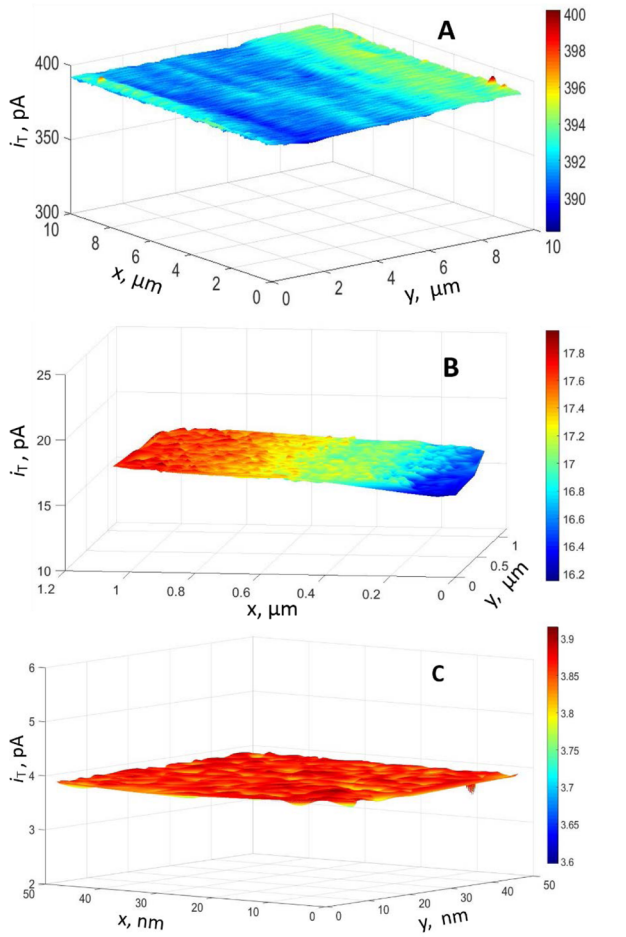

Figure 5. SECM images of HOPG modified with TPD: (A) 10 × 10 μm^2 image obtained with a 1.5 μm radius Pt tip, (B) 1 × 1 μm^2 image obtained with an 80 nm tip, and (C) 50 × 50 nm^2 image obtained with a 16 nm tip. The mediator was 1 mM Fc. For other parameters, see Figure 4.

reaction was hindered so strongly that only a pure negative feedback was obtained in SECM experiments (not shown). Figure 4 shows the approach curve obtained at the TPD-modified HOPG with the Fc mediator. The tip radius, a = 1.2 μm, was obtained from the diffusion-limiting current ($i_{T,\infty}$) in the steady-state voltammogram (inset in Figure 4) using eq 2

$$i_{T,\infty} = 4FDca \quad (2)$$

where F is the Faraday constant, D = 7.8 × 10^{-6} cm^2/s[33] and c = 1 mM are the diffusion coefficient and the concentration of Fc.

The experimental approach curve (symbols in Figure 4) was fitted to the theory (eq 6 in ref 36) to extract the effective rate constant for the Fc regeneration at the substrate, k_{eff} = 0.22 cm/s. This value is about 2 orders of magnitude smaller than the lower limit for the formal rate constant ($k^{o\prime}$ > 17 cm/s) measured recently for a ferrocene species, (ferrocenylmethyl)-trimethylammonium, at HOPG in aqueous KCl solution.[37] Keeping in mind that the k_{eff} value extracted from Figure 4 corresponds to E_S = −0.1 V versus Ag/AgCl, which is about 0.2 V more negative than the formal potential of Fc (see inset in Figure 4), this rate constant is at least 5000 times lower than the value expected at the bare HOPG surface.

DOI: 10.1021/acs.langmuir.5b03858
Langmuir 2016, 32, 2500−2508

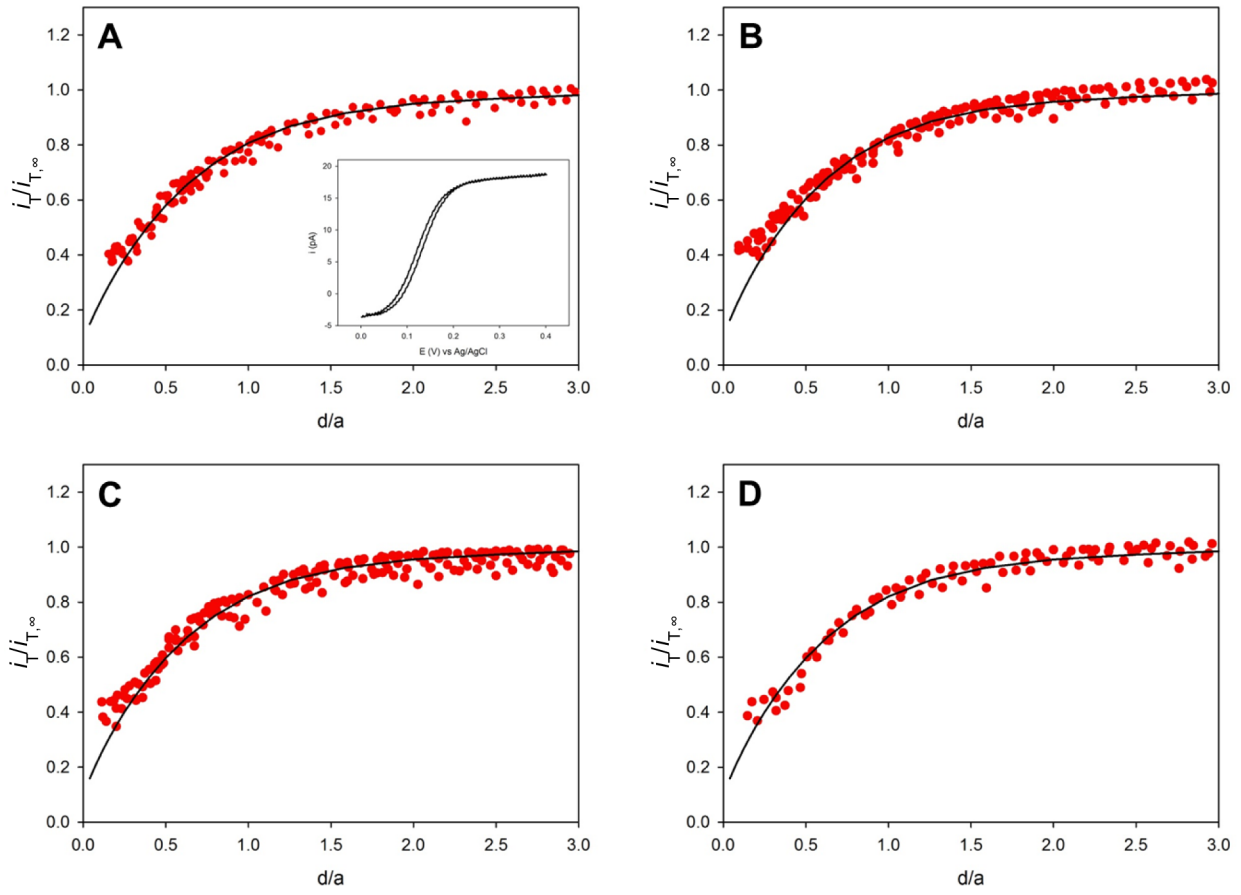

Figure 6. Experimental (symbols) SECM approach curves at the TPD-modified HOPG substrate fitted to the theory (solid curves[36]). The approach curves were obtained at four different spots located ~10 μm apart from each other. The effective rate constants extracted from the fit, k_{eff},: (A, C, and D) 0.17 cm/s and (B) 0.18 cm/s. The inset shows a steady-state voltammogram of Fc at the same tip electrode. a = 60 nm. For other parameters, see Figure 4.

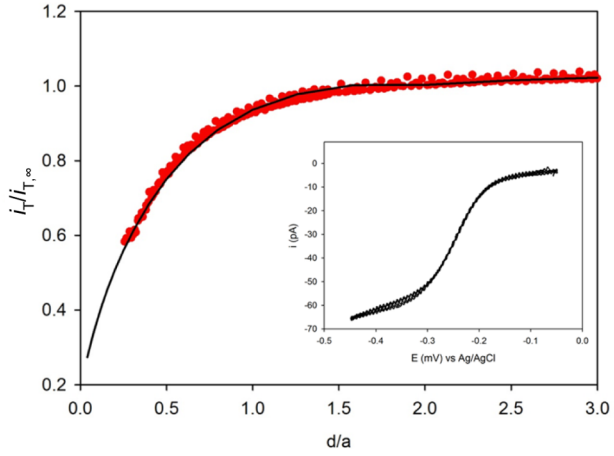

Figure 7. Experimental (symbols) SECM approach curve at the TPD-modified HOPG substrate obtained in 1 mM solution of $Ru(NH_3)_6Cl_3$ and fitted to the theory (solid curve[36]). E_S = 0.1 V, and E_T = −0.45 V. The inset shows a steady-state voltammogram of the $Ru(NH_3)_6^{3+}$ reduction at the same tip electrode. Scan rate, v = 50 mV/s. a = 250 nm.

The SECM images of TPD-modified HOPG substrates obtained with micrometer-sized tips and Fc mediator were featureless, corresponding to the uniform electrochemical reactivity of the modified substrate on the micrometer scale (Figure 5A). This observation also points to the absence of large (i.e., micrometer- or sub-micrometer-sized) defects in the film that would be observable in such images.

Four approach curves to the TPD-modified HOPG substrate in Figure 6 were obtained under the same experimental conditions as in Figure 4, except for a much smaller tip electrode (a = 60 nm). Although the shape of these curves is markedly different from the curve in Figure 4 (i.e., the current decreases with decreasing d), the extracted effective rate constants (0.17−0.18 cm/s) are similar to the 0.22 cm/s value found with a micrometer-sized tip. These data along with very similar k_{eff} values found at four different spots suggest that the film reactivity is uniform on the spatial scale of tens of nanometers. This finding is consistent with the 1 × 1 μm^2 image obtained with the 80 nm radius tip that shows uniformly negative feedback (Figure 5B; $i_{T,\infty}$ = 24 pA) and no evidence of defects with the size comparable to the tip radius.

A much higher resolution 50 × 50 nm^2 HOPG/TPD image (Figure 5C) obtained with a 16 nm tip is flat and featureless. The tip current was very stable, with the maximum variation of <0.2 pA, and showed a significant negative feedback ($i_{T,\infty}$ = 4.8 pA). With the tip of this size, one should be able to detect ~2−3 nm radius defects.[38] No such features can be seen in Figure 5C and several other images obtained with similarly sized tips (not shown). The same conclusion can be drawn from the 1 × 1 μm^2 non-contact AFM image of the same film (Figure 2B), showing the film roughness of ≤1 nm and no identifiable defects.

DOI: 10.1021/acs.langmuir.5b03858
Langmuir 2016, 32, 2500−2508

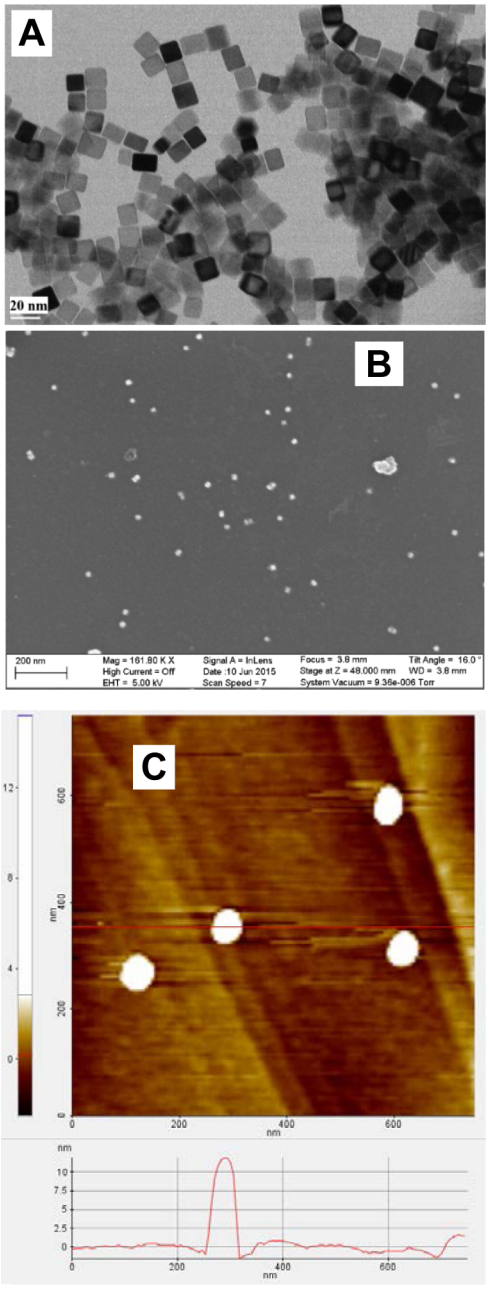

Figure 8. (A) TEM image of synthesized Pd nanocubes dried on a carbon-coated copper grid and (B) SEM and (C) AFM images of Pd nanocubes anchored to the TPD film. The red line in panel C corresponds to the shown cross-section.

The apparent rate constant for $Ru(NH_3)_6^{3/2+}$ extracted from the fit of the experimental approach curve (symbols in Figure 7) to the theory (solid line) was 0.065 versus ~0.2 cm/s for Fc. This lower k_{eff} was obtained at ~50 mV higher overpotential value, as compared to that in Figures 4 and 6. The formal heterogeneous rate constants measured for $Ru(NH_3)_6^{3+}$ reduction at either Pt or Au nanoelectrodes were somewhat higher than that of Fc oxidation.[33] Overall, the blocking effect of the TPD film toward the $Ru(NH_3)_6^{3/2+}$ mediator was somewhat stronger than that measured with the Fc species.

At the level of a few nanometers lateral resolution attained in this work, the rate of charge propagation through the TPD film appears to be uniform and no individual defects or pores could be detected. Unlike charged aryldiazonium multilayers

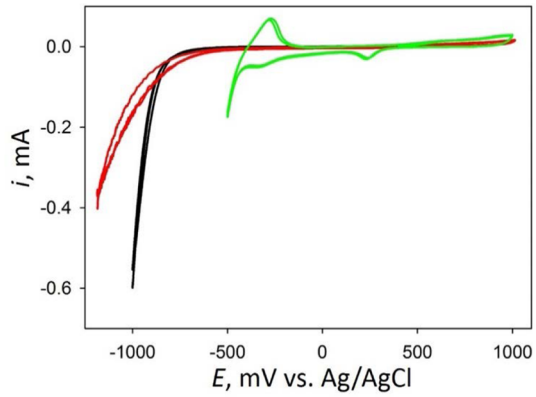

Figure 9. CVs obtained in 1 M $HClO_4$ at bare HOPG (black), HOPG modified with TPD (red), and the same electrode with attached Pd nanocubes (green).

investigated in previous studies,[7,9] TPD films are electrically neutral and the origin of ET blocking is not electrostatic. The comparable rate constants measured for a hydrophilic $[Ru(NH_3)_6^{3+}]$ and more hydrophobic (Fc) species, as opposed to immeasurably slow reduction of another hydrophilic ion $[Fe(CN)_6^{3+}]$, suggest that the hydrophilicity of the mediator is not a major factor determining the magnitude of the blocking effect.

The decreased surface area available for ET at modified HOPG should result in the lower effective heterogeneous rate constant, $k_{eff} = (1 - \theta)k_f$, where θ is the surface coverage and k_f is the rate constant of the mediator regeneration at bare HOPG biased at the same potential. For the k_{eff} to be about 3−4 orders of magnitude smaller than k_f [as measured above for $Ru(NH_3)_6^{3+}$ and Fc], the surface coverage has to be higher than 99.9%. Such a coverage can be expected for highly ordered films (e.g., thiol monolayers on Au) rather than aryl multilayers, which are known to be less compact. The observed blocking effect is likely increased by slow charge propagation through the film, whose rate can be expressed by the permeability coefficient, $P = KD_f/l_f$, where D_f is the diffusion coefficient in the film, K is the solution-to-film partition coefficient of the redox species, and l_f is the film thickness. Under steady-state conditions, eq 3 (instead of eq 1 applicable to a blocking monolayer) can be used to describe the combined effects of the decreased surface area available for ET and slow charge propagation through the film on the effective rate constant measured by SECM (k_{eff})[39]

$$1/k_{eff} = 1/((1 - \theta)k_f) + 2/P \quad (3)$$

where the factor 2 reflects the fact that the mediator has to cross the film twice to produce the SECM feedback.

Because of the slow physical diffusion of ions in the film, D_f is likely to reflect the electron hopping rate,[12] which is determined by the self-exchange rate constant (k_{ex}).[40] Although the K, D_f, and l_f values required for the evaluation of P are not available, the magnitude of the film blocking effect toward different mediators can be understood from semi-quantitative analysis of eq 3. For $Fe(CN)_6^{3/4-}$, both k° and k_{ex} (240 M^{-1} s^{-1} [41]) are much smaller than for two other redox mediators used in this study, resulting in an immeasurably slow k_{eff}. The aforementioned somewhat stronger blocking effect of the TPD film toward the $Ru(NH_3)_6^{3/2+}$ mediator than toward Fc species should be related to the difference in their k_{ex} values [i.e., 3×10^3 M^{-1} s^{-1} for $Ru(NH_3)_6^{3/2+}$ [42] and 9×10^6 M^{-1} s^{-1} for

DOI: 10.1021/acs.langmuir.5b03858
Langmuir 2016, 32, 2500−2508

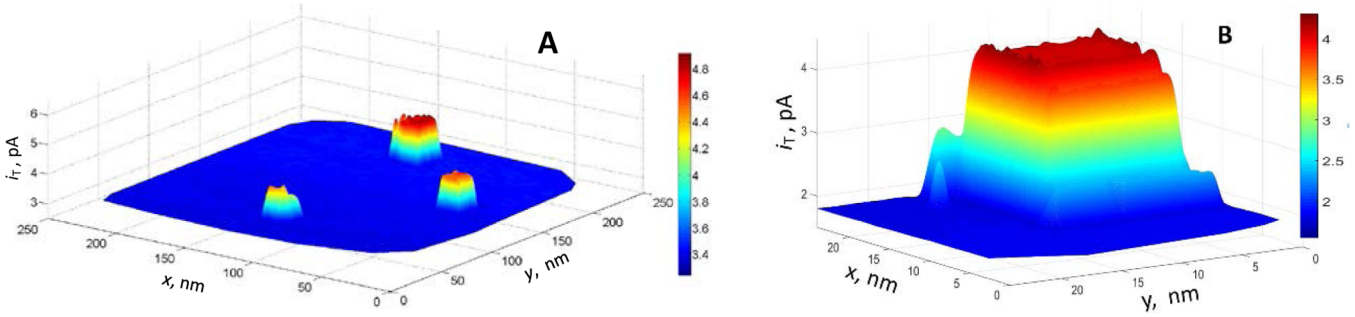

Figure 10. SECM images of HOPG with Pd nanocubes attached to the electrografted TPD film: (A) 200 × 200 nm^2 image (60 lines, 60 pixels per line) obtained with a 13 nm radius Pt tip and (B) 25 × 25 nm^2 image (25 lines, 50 pixels per line) of a Pd nanocube obtained with a 10 nm radius Pt tip. For other parameters, see Figure 4.

$Fc^{+/0}$ [43]. The faster k_{ex} of $Fc^{+/0}$ corresponds to the faster electron hopping rate and, thus, larger permeability coefficient of this species through the TPD film.

SECM Imaging of Pd Nanocubes Attached to a HOPG/TPD Substrate. A TEM image in Figure 8A shows that Pd nanocubes employed in electrochemical experiments were reasonably uniform, with the edge length of 14 ± 2 nm.

Unlike our previous experiments with AuNPs electrostatically attached to negatively charged polyphenylene films,[24,25] Pd nanocubes were anchored to the HOPG/TPD surface by thiol groups. A SEM image in Figure 8B shows that this immobilization protocol produced mostly non-aggregated and well-separated nanocubes. Although the spatial resolution in Figure 8B is not sufficiently high to determine the exact size of the particles, it appears to be under 20 nm. The corresponding AFM image (Figure 8C) also shows well-separated individual nanoparticles. The apparent nanoparticle height of ~12 nm is close to that found from TEM images, suggesting that the cubes may only be slightly buried in the polyphenylene layer, while a significantly larger lateral nanoparticle size (~60 nm) in the image is due to the tip convolution effect, as discussed earlier.[24,44] The nanoparticles in Figure 8C do not look rectangular because of the limited lateral resolution.

The nanocubes were electrically connected to the HOPG surface and showed catalytic activity toward proton reduction, as seen from CVs recorded in perchloric acid (Figure 9). The hydrogen adsorption and oxygen peaks are evident in CV obtained at the electrode decorated with Pd nanocubes (green curve) but not in those obtained at bare HOPG (black curve) and HOPG modified with the TPD film (red curve). The ~500 mV shift of the hydrogen evolution wave is very large, keeping in mind a low density of Pd nanocubes on the HOPG surface and the presence of the CTAB capping agent, which is known to diminish the catalytic activity of nanoparticles.

The 200 × 200 nm^2 constant-height SECM image obtained with a 13 nm radius tip in a 1 mM Fc solution (Figure 10A) shows positive feedback over three Pd nanocubes and negative feedback over the TPD film ($i_{T,\infty}$ = 3.9 pA). As discussed earlier,[24] significant positive feedback obtained at an unbiased macroscopic substrate with a low density of anchored nanoparticles (Figure 1B) points to efficient ET between the Pd nanocubes and HOPG surface.

A slightly smaller tip (a = 10 nm) was used to zoom in on a single Pd cube (Figure 10B). The 25 × 25 nm image shows a parallelepipedal nanoparticle with ~13 × 13 nm base in a very good agreement with the TEM images of similar nanocubes, thus suggesting that SECM can be used for characterizing the geometry of relatively small (i.e., 10−20 nm) nanoparticles. An important potential advantage of this approach is the possibility of using SECM for kinetic experiments at the same nanoparticle[24] after characterizing its geometry.

Similar to our previous experiments with spherical Au nanoparticles,[24] the lateral resolution of SECM imaging in Figure 10B is significantly higher than that in the AFM image (Figure 8B) obtained with a typical commercial probe. The image of the cube in Figure 10B is also much sharper than it can be expected to look according to the existing SECM theory. Our COMSOL simulations (Supporting Information) indicate that no sharp edges or corners should be visible in the image of such a nanoparticle obtained with a 10 nm tip, and the top surface of the cube should not look flat. The tentative explanation is that the images of metal nanoparticles obtained with small (~10 nm) SECM tips are often affected by tunneling between the tip and the nanoparticle. This effect may account for very sharp features in Figure 10 that would not be possible to see from variations in the diffusion current to the tip. Although the imaging mechanism is not completely clear at this time, the shape and size of the nanoparticles in Figure 10 are in very good agreement with TEM results, thus supporting the validity these images. Experiments and modeling are currently underway to better understand this phenomenon that can further improve spatial resolution of SECM imaging.

■ CONCLUSION

We used SECM for nanoscale characterization of the barrier properties of the TPD multilayers electrografted onto HOPG. The effective rate constants extracted from approach curves obtained with micrometer- and nanometer-sized SECM tips positioned over different substrate areas suggested that the TPD film reactivity is spatially uniform. The micro- and nanoscale SECM images of the HOPG/TPD substrates also showed uniform film reactivity. No pinhole defects could be detected using a tip as small as 16 nm radius, thus indicating that the TPD films contain no pores larger than ~2−3 nm radius. By considering the combination of the decreased surface area available for ET and slow charge propagation through the film, one can explain the relative magnitude of the blocking effect of the TPD multilayer toward different redox mediators [$Fe(CN)_6^{3/4-}$, Fc^+/Fc, and $Ru(NH_3)_6^{3/2+}$].

The uniformly negative feedback in SECM images of TPD films and current−distance curves obtained with nanometer-sized tips is essential for imaging of and kinetic studies at the attached metal nanoparticles. The charge transfer through TPD films is too slow to contribute to the tip current during the experiments at the attached nanoparticles, employing 10−20

DOI: 10.1021/acs.langmuir.5b03858
Langmuir 2016, 32, 2500−2508

nm radius tips. Pd nanocubes were anchored to the TPD-modified HOPG surface via thiol groups. This versatile strategy should be useful for binding Au, Pd, or Pt nanoparticles. The Pd nanocubes with the 14 nm edge length were imaged by SECM. Similarly sized spherical Au particles had recently been visualized by SECM, and their radii were determined from the approach curves.[25] Here, we showed that SECM can also be used to characterize the shape of non-spherical nanoparticles. An advantage of this approach is that, after determination of the shape and size of a specific nanoparticle, the SECM tip can probe electrocatalytic processes occurring at its surface[24] and investigate the effects of the size, shape, and attachment on the nanoparticle catalytic activity.

■ ASSOCIATED CONTENT

Supporting Information

The Supporting Information is available free of charge on the ACS Publications website at DOI: 10.1021/acs.langmuir.5b03858.

Simulated SECM images of a nanocube, scheme of the simulation domain and related parameter values, formulation of the diffusion problem for SECM of a nanocube, and COMSOL model report (PDF)

■ AUTHOR INFORMATION

Corresponding Authors

*E-mail: hmatsui@hunter.cuny.edu.
*E-mail: mmirkin@qc.cuny.edu.

Notes

The authors declare no competing financial interest.

■ ACKNOWLEDGMENTS

The support of this work by the National Science Foundation (CHE-1300158) and Air Force Office of Scientific Research (AFOSR) Multidisciplinary Research Program of the University Research Initiative (MURI) FA9550-14-1-0003 (M.V.M.), and the National Institute on Minority Health and Health Disparities of National Institutes of Health (MD007599) and the Division of Materials Sciences and Engineering, Office of Basic Energy Sciences, United States Department of Energy, under Award DE-FG-02-01ER45935 (to H.M.), is gratefully acknowledged.

■ REFERENCES

(1) Delamar, M.; Hitmi, R.; Pinson, J.; Savéant, J. M. Covalent modification of carbon surfaces by grafting of functionalized aryl radicals produced from electrochemical reduction of diazonium salts. *J. Am. Chem. Soc.* **1992**, *114*, 5883−5884.

(2) Bélanger, D.; Pinson, J. Electrografting: a powerful method for surface modification. *Chem. Soc. Rev.* **2011**, *40*, 3995−4048.

(3) Combellas, C.; Delamar, M.; Kanoufi, F.; Pinson, J.; Podvorica, F. I. Spontaneous grafting of iron surfaces by reduction of aryldiazonium salts in acidic or neutral aqueous solution. Application to the protection of iron against corrosion. *Chem. Mater.* **2005**, *17*, 3968−3975.

(4) Sayed, S. Y.; Bayat, A.; Kondratenko, M.; Leroux, Y.; Hapiot, P.; McCreery, R. L. Bilayer molecular electronics: all-carbon electronic junctions containing molecular bilayers made with "click" chemistry. *J. Am. Chem. Soc.* **2013**, *135*, 12972−12975.

(5) Liu, G.; Böcking, T.; Gooding, J. J. Diazonium salts: Stable monolayers on gold electrodes for sensing applications. *J. Electroanal. Chem.* **2007**, *600*, 335−344.

(6) Pognon, G.; Brousse, T.; Demarconnay, L.; Bélanger, D. Performance and stability of electrochemical capacitor based on anthraquinone modified activated carbon. *J. Power Sources* **2011**, *196*, 4117−4122.

(7) Schauff, S.; Ciorca, M.; Laforgue, A.; Bélanger, D. Electron Transfer Processes at Aryl-Modified Glassy Carbon Electrode. *Electroanalysis* **2009**, *21*, 1499−1504.

(8) Downard, A. J.; Prince, M. J. Barrier properties of organic monolayers on glassy carbon electrodes. *Langmuir* **2001**, *17*, 5581−5586.

(9) Griveau, S.; Aroua, S.; Bediwy, D.; Cornut, R.; Lefrou, C.; Bedioui, F. Spontaneous adsorbed layers of 4-nitrobenzenediazonium salt on gold and glassy carbon: Local characterization by SECM and electron-transfer kinetics evaluation. *J. Electroanal. Chem.* **2010**, *647*, 93−96.

(10) Brooksby, P. A.; Downard, A. J. Electrochemical and atomic force microscopy study of carbon surface modification via diazonium reduction in aqueous and acetonitrile solutions. *Langmuir* **2004**, *20*, 5038−5045.

(11) Ceccato, M.; Bousquet, A.; Hinge, M.; Pedersen, S. U.; Daasbjerg, K. Using a mediating effect in the electroreduction of aryldiazonium salts to prepare conducting organic films of high thickness. *Chem. Mater.* **2011**, *23*, 1551−1557.

(12) March, G.; Reisberg, S.; Piro, B.; Pham, M.-C.; Fave, C.; Noël, V. Hydroxynaphthoquinone Ultrathin Films Obtained by Diazonium Electroreduction: Toward Design of Biosensitive Electroactive Interfaces. *Anal. Chem.* **2010**, *82*, 3523−3530.

(13) Noël, J.-M.; Sjöberg, B. a.; Marsac, R.; Zigah, D.; Bergamini, J.-F.; Wang, A.; Rigaut, S.; Hapiot, P.; Lagrost, C. Flexible strategy for immobilizing redox-active compounds using in situ generation of diazonium salts. Investigations of the blocking and catalytic properties of the layers. *Langmuir* **2009**, *25*, 12742−12749.

(14) Zigah, D.; Noël, J.-M.; Lagrost, C.; Hapiot, P. Charge Transfer between Electroactive Species Immobilized on Carbon Surfaces by Aryl Diazonium Reduction. SECM Investigations. *J. Phys. Chem. C* **2010**, *114*, 3075−3081.

(15) Hauquier, F.; Matrab, T.; Kanoufi, F.; Combellas, C. Local direct and indirect reduction of electrografted aryldiazonium/gold surfaces for polymer brushes patterning. *Electrochim. Acta* **2009**, *54*, 5127−5136.

(16) Bernard, M.-C.; Chaussé, A.; Cabet-Deliry, E.; Chehimi, M. M.; Pinson, J.; Podvorica, F.; Vautrin-Ul, C. Organic layers bonded to industrial, coinage, and noble metals through electrochemical reduction of aryldiazonium salts. *Chem. Mater.* **2003**, *15*, 3450−3462.

(17) Mirkin, M. V.; Arca, M.; Bard, A. J. Scanning electrochemical microscopy. 22. Examination of thin solid silver (I) bromide films: ion diffusion in the film and heterogeneous kinetics at the film/solution interface. *J. Phys. Chem.* **1993**, *97*, 10790−10795.

(18) Forouzan, F.; Bard, A. J.; Mirkin, M. V. Voltammetric and Scanning Electrochemical Microscopic Studies of the Adsorption Kinetics and Self-Assembly of n-Alkanethiol Monolayers on Gold. *Isr. J. Chem.* **1997**, *37*, 155−163.

(19) Liu, B.; Bard, A. J.; Mirkin, M. V.; Creager, S. E. Electron transfer at self-assembled monolayers measured by scanning electrochemical microscopy. *J. Am. Chem. Soc.* **2004**, *126*, 1485−1492.

(20) Yamada, H.; Ogata, M.; Koike, T. Scanning electrochemical microscope observation of defects in a hexadecanethiol monolayer on gold with shear force-based tip-substrate positioning. *Langmuir* **2006**, *22*, 7923−7927.

(21) Ghilane, J.; Hauquier, F.; Fabre, B.; Hapiot, P. Scanning electrochemical microscopy investigations of monolayers bound to p-type silicon substrates. *Anal. Chem.* **2006**, *78*, 6019−6025.

(22) Lhenry, S.; Jalkh, J.; Leroux, Y. R.; Ruiz, J.; Ciganda, R.; Astruc, D.; Hapiot, P. Tunneling Dendrimers. Enhancing Charge Transport through Insulating Layer Using Redox Molecular Objects. *J. Am. Chem. Soc.* **2014**, *136*, 17950−17953.

(23) White, H. S.; Kanoufi, F. In Imaging Molecular Transport across Membranes. In *Scanning Electrochemical Microscopy*, 2nd ed.; Bard, A.

DOI: 10.1021/acs.langmuir.5b03858
Langmuir 2016, 32, 2500−2508

J., Mirkin, M. V., Eds.; CRC Press: Boca Raton, FL, 2012, Chapter 9, pp 233−274, DOI: 10.1201/b11850-10.
(24) Sun, T.; Yu, Y.; Zacher, B. J.; Mirkin, M. V. Scanning Electrochemical Microscopy of Individual Catalytic Nanoparticles. *Angew. Chem., Int. Ed.* **2014**, *53*, 14120−14123.
(25) Yu, Y.; Sun, T.; Mirkin, M. V. Scanning Electrochemical Microscopy of Single Spherical Nanoparticles: Theory and Particle Size Evaluation. *Anal. Chem.* **2015**, *87*, 7446−7453.
(26) Amemiya, S. Nanoscale Scanning Electrochemical Microscopy. In *Electroanalytical Chemistry*; Bard, A. J., Zoski, C. G., Eds.; CRC Press (Taylor and Francis Group): Boca Raton, FL, 2015; Vol. *26*, pp 1−72, DOI: 10.1201/b19196-2.
(27) Oja, S. M.; Fan, Y.; Armstrong, C. M.; Defnet, P.; Zhang, B. Nanoscale Electrochemistry Revisited. *Anal. Chem.* **2016**, *88*, 414−430.
(28) O'Connell, M. A.; Wain, A. J. Mapping Electroactivity at Individual Catalytic Nanostructures Using High-Resolution Scanning Electrochemical−Scanning Ion Conductance Microcopy. *Anal. Chem.* **2014**, *86*, 12100−12107.
(29) O'Connell, M. A.; Lewis, J. R.; Wain, A. J. Electrochemical imaging of hydrogen peroxide generation at individual gold nanoparticles. *Chem. Commun.* **2015**, *51*, 10314−10317.
(30) Huang, K.; Anne, A.; Bahri, M. A.; Demaille, C. Probing Individual Redox PEGylated Gold Nanoparticles by Electrochemical−Atomic Force Microscopy. *ACS Nano* **2013**, *7*, 4151−4163.
(31) Nault, L.; Taofifenua, C.; Anne, A.; Chovin, A.; Demaille, C.; Besong-Ndika, J.; Cardinale, D.; Carette, N.; Michon, T.; Walter, J. Electrochemical Atomic Force Microscopy Imaging of Redox-Immunomarked Proteins on Native Potyviruses: From Subparticle to Single-Protein Resolution. *ACS Nano* **2015**, *9*, 4911−4924.
(32) Wei, Z.; Matsui, H. Rational strategy for shaped nanomaterial synthesis in reverse micelle reactors. *Nat. Commun.* **2014**, *5*, 3870.
(33) Sun, P.; Mirkin, M. V. Kinetics of electron-transfer reactions at nanoelectrodes. *Anal. Chem.* **2006**, *78*, 6526−6534.
(34) Nioradze, N.; Chen, R.; Kim, J.; Shen, M.; Santhosh, P.; Amemiya, S. Origins of Nanoscale Damage to Glass-Sealed Platinum Electrodes with Submicrometer and Nanometer Size. *Anal. Chem.* **2013**, *85*, 6198−6202.
(35) Nogala, W.; Velmurugan, J.; Mirkin, M. V. Atomic force microscopy of electrochemical nanoelectrodes. *Anal. Chem.* **2012**, *84*, 5192−5197.
(36) Wei, C.; Bard, A. J.; Mirkin, M. V. Scanning electrochemical microscopy. 31. Application of SECM to the study of charge transfer processes at the liquid/liquid interface. *J. Phys. Chem.* **1995**, *99*, 16033−16042.
(37) Nioradze, N.; Chen, R.; Kurapati, N.; Khvataeva-Domanov, A.; Mabic, S.; Amemiya, S. Organic Contamination of Highly Oriented Pyrolytic Graphite as Studied by Scanning Electrochemical Microscopy. *Anal. Chem.* **2015**, *87*, 4836−4843.
(38) Bard, A. J.; Mirkin, M. V.; Unwin, P. R.; Wipf, D. O. Scanning electrochemical microscopy. 12. Theory and experiment of the feedback mode with finite heterogeneous electron-transfer kinetics and arbitrary substrate size. *J. Phys. Chem.* **1992**, *96*, 1861−1868.
(39) Andrieux, C. P.; Savéant, J.-M Catalysis at Redox Polymer Coated Electrodes. In *Molecular Design of Surfaces*; Murray, R. W., Ed.; John Wiley & Sons: New York, 1992; p 207.
(40) Murray, R. W. Chemically Modified Electrodes. In *Electroanalytical Chemistry*; Bard, A. J., Ed.; Marcel Dekker: New York, 1984; Vol. *13*, pp 191−368.
(41) Zahl, A.; van Eldik, R.; Swaddle, T. W. Cation-independent electron transfer between ferricyanide and ferrocyanide ions in aqueous solution. *Inorg. Chem.* **2002**, *41*, 757−764.
(42) Marcus, R. A.; Sutin, N. Electron transfers in chemistry and biology. *Biochim. Biophys. Acta, Rev. Bioenerg.* **1985**, *811*, 265−322.
(43) Fawcett, W. R.; Opallo, M. The kinetics of heterogeneous electron transfer reaction in polar solvents. *Angew. Chem., Int. Ed. Engl.* **1994**, *33*, 2131−2143.
(44) Zheng, J.; Zhu, Z.; Chen, H.; Liu, Z. Nanopatterned assembling of colloidal gold nanoparticles on silicon. *Langmuir* **2000**, *16*, 4409−4412.

DOI: 10.1021/acs.langmuir.5b03858
Langmuir 2016, 32, 2500−2508